Supplementary Information

The quest for (and some surprises in) the determination of the Gaussian modulus and edge tension of 2D materials—from graphene to lipid bilayers

Matthew Zelisko, Fatemeh Ahmadpoor, Huajian Gao, and Pradeep Sharma

1. Mathematical preliminaries

Consider an open elastic membrane, having a smooth and orientable surface Ω, enclosed by a space curve $\partial\Omega$ that represents the edge of the surface. Let $\mathbf{n}$ be the normal vector field on Ω. Then the curvature tensor $\mathbf{L}$ and mean and Gaussian curvatures (H, K) can be obtained as:

$$\begin{aligned} &\mathbf{L} = -\nabla_S \mathbf{n}, \\ &H = -\frac{1}{2}\mathrm{div}_S\,\mathbf{n}, \quad K = \frac{1}{2}\left((\mathrm{tr}\,\mathbf{L})^2 - \mathrm{tr}(\mathbf{L}^2)\right) \end{aligned} \tag{1}$$

where ∇_S and div_S correspond to surface gradient and surface divergence operators. To explain the surface operators, let surface projection tensor be defined as:

$$\mathbf{P} = \mathbf{I} - \mathbf{n} \otimes \mathbf{n}, \tag{2}$$

where $\mathbf{I}$ is the identity tensor. The surface gradient, surface Laplacian and surface divergence of a scalar field f and a vector field $\mathbf{g}$ can then be defined in terms of $\mathbf{P}$ and their smooth extensions f^e and $\mathbf{g}^e$ as[1]:

$$\begin{aligned} &\nabla_S f = \mathbf{P}\nabla f^e, \qquad \nabla_S \mathbf{g} = (\nabla \mathbf{g}^e)\mathbf{P}, \\ &\mathrm{div}_S \mathbf{g} = \mathbf{P} \cdot \nabla \mathbf{g}^e, \qquad \Delta_S f = \mathrm{div}_S(\nabla_S f) \end{aligned} \tag{3}$$

Let $\mathbf{e}$ be the tangent unit vector of the edge curve $\partial\Omega$. Then $\nu = \mathbf{e} \times \mathbf{n}$ would be tangent to the surface Ω and normal the edge curve. The total curvature vector of the edge curve is obtained by taking the derivative of $\mathbf{e}$ with respect to the edge's arc length:

$$\kappa = \mathbf{e}' = \kappa_n \mathbf{n} - \kappa_g \nu \tag{4}$$

where κ_n and κ_g are the component of the curvature along the normal vectors of the surface and the edge, respectively.

2. Elasticity of a surface with open edge

Let ψ and ϕ be the areal energy density of the surface and lineal energy density of the edge of the surface, respectively. Then the total elastic energy can be split into two parts as:

$$F = \int_{\Omega} \psi + \int_{\partial\Omega} \phi. \tag{5}$$

where ψ, up to quadratic order is

$$\overline{\psi} = \frac{1}{2}\kappa_b H^2 + \kappa_G K. \tag{6}$$

Also, the edge energy— as proposed by Biria et al.[1]—is geometry dependent. In the absence of the edge torsion, the edge energy density can be expressed as [1]:

$$\phi = \phi_0 + \bar{\phi}(\kappa_n, \kappa_g), \tag{7}$$

where ϕ_0 is a constant and is the so-called edge(line) tension. Up to a quadratic order, ϕ can be expressed as [2]:

$$\phi = \phi_0 + \frac{1}{2}\kappa_s(\kappa_n^2 + \kappa_g^2) + \cdots, \tag{8}$$

where κ_s can be defined as the bending *modulus* of the edge.

Now, suppose that the possible deformations are normal to the surface: $\mathbf{U} = h\mathbf{n}$. Minimization of the total elastic energy, in the absence of external forces and moments[1], then leads to the following ground-state (zero Kelvin) Euler-Lagrange equations:

$$\begin{aligned}&\psi_H(2H^2 - K) + \frac{1}{2}\triangle_S\psi_H + 2\psi_K HK + 2\triangle_S(\psi_K H)\\ &- \mathrm{div}_S(\mathbf{L}\nabla_{\mathbf{S}}\psi_{\mathbf{K}}) - 2(\nabla_S H)\cdot(\nabla_S\psi_K) - 2\psi_K\triangle_S H - 2\psi H = 0,\end{aligned} \tag{9}$$

The corresponding boundary conditions on the edge are given by[1]:

$$\begin{aligned}&(\mathbf{L}\nabla_S\psi_K - \frac{1}{2}\nabla_S\psi_H - 2H\nabla_S\psi_K)\cdot\nu + \bar{\phi}_{\kappa_n}\kappa_n^2\\ &\qquad + \bar{\phi}_{\kappa_g}\kappa_n\kappa_g - \phi\kappa_n - \bar{\phi}''_{\kappa_n} = 0\end{aligned} \tag{10a}$$

$$\frac{1}{2}\psi_H + \psi_K\kappa_n + \bar{\phi}_{\kappa_n}\kappa_g - \bar{\phi}_{\kappa_g}\kappa_n = 0, \tag{10b}$$

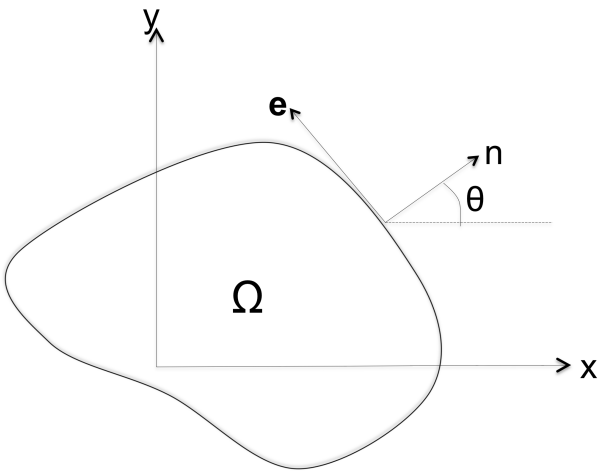

Figure 1: Schematic of a planar surface embedded in domain Ω, having a closed edge $\partial\Omega$. The unit tangent and normal vectors of the edge curve are shown. Also θ is defined as the angle between the normal vector to the edge and the x axis.

for free edges and

$$h = 0, \qquad \nabla_S h \cdot \nu = 0, \tag{11}$$

for constrained edges.

Now let Ω be on the xy plane occupying an area of A. Within linearized approximations the mean and Gaussian curvatures are expressed as:

$$H = -\frac{1}{2}\nabla^2 h, \qquad K = h_{xx}h_{yy} - (h_{xy})^2 \tag{12}$$

Further, under the assumption of zero tangential deformations, the curvatures of the edge can be obtained as:

$$\kappa_n = \frac{\partial^2 h}{\partial s^2}, \qquad \kappa_g = 0 \tag{13}$$

where s is the arc-length of the edge curve. Let θ (as shown in Figure. 1) be the angle between the normal of the edge and the x axis.

Depending on clamped or free edges, one can specify different set of

boundary conditions. For clamped edge, one need to set:

$$\begin{aligned} h(\mathbf{x}) &:= 0, \qquad \mathbf{x} \in \partial\Omega \\ \frac{\partial h(\mathbf{x})}{\partial n} &:= 0, \qquad \mathbf{x} \in \partial\Omega \end{aligned} \tag{14}$$

while for free edges, we obtain:

$$\begin{aligned} &\kappa_b \frac{\partial(\nabla^2 h)}{\partial n} + \kappa_G \frac{\partial}{\partial s}\Big\{ \sin\theta\cos\theta(\frac{\partial^2 h}{\partial y^2} - \frac{\partial^2 h}{\partial x^2})\Big\} \\ &+ \kappa_G \frac{\partial}{\partial s}\Big\{(\sin^2\theta - \cos^2\theta)\frac{\partial^2 h}{\partial y \partial x}\Big\} + \phi_0 \frac{\partial^2 h}{\partial s^2} - \kappa_s \frac{\partial^4 h}{\partial s^4} := 0, \\ &\qquad\qquad \mathbf{x} \in \partial\Omega \\ &\kappa_b \nabla^2 h - \kappa_G \left(2\sin\theta\cos\theta \frac{\partial^2 h}{\partial x \partial y} - \sin^2\theta \frac{\partial^2 h}{\partial x^2}\right. \\ &\qquad\qquad \left. - \cos^2\theta \frac{\partial^2 h}{\partial y^2}\right) := 0, \\ &\qquad\qquad \mathbf{x} \in \partial\Omega \end{aligned} \tag{15}$$

3. Statistical mechanics of elastic membranes with open edges

Statistical mechanics of elastic membranes is extensively studied in the literature. In the majority of these work, the membrane—occupying a domain of $\Omega^{\mathrm{P}} = (0, L)^2$ in the xy plane— is assumed to be large enough that the effects of boundary conditions are negligible; i.e. the energy at the boundary in is hence neglected. Accordingly, a periodic boundary condition is assumed in all the directions. In this manner, due to Gauss-Bonnet theorem, the integration of the Gaussian curvature of a membrane, without edge is constant. Hence, the elastic energy is described solely in terms of the mean curvature. For periodic boundary conditions the out-of-plane deformation of the membrane can be easily described in Fourier space as:

$$h(\mathbf{x}) = \sum_{\mathbf{q}\in\mathbb{K}} \bar{h}_{\mathbf{q}} \mathrm{e}^{\imath \mathbf{q}\cdot\mathbf{x}} \tag{16}$$

in which to avoid divergencies, we introduce cut-off lengths for wave vectors as: $q := |\mathbf{q}| \in [q_{\min}, q_{\max}]$, i.e.

$$\mathbb{K} = \big\{\mathbf{q} : \mathbf{q} = \frac{2\pi}{L}(\nu_x, \nu_y), \nu_x, \nu_y \in \mathbb{Z}, |\mathbf{q}| \in [q_{\min}, q_{\max}]\big\}$$

Substituting the expansion (16) in the *linearized* elastic energy gives us:

$$\begin{aligned} U_{\Omega^{\mathrm{P}}} &= \frac{L^2}{2} \sum_{\mathbf{q},\mathbf{q}' \in \mathbb{K}} \kappa_b |\mathbf{q}|^2 |\mathbf{q}'|^2 \bar{h}_{\mathbf{q}} \bar{h}_{\mathbf{q}'} \int_{\Omega^{\mathrm{P}}} \mathrm{e}^{\imath(\mathbf{q}+\mathbf{q}')\cdot\mathbf{x}} \\ &= \frac{L^2}{2} \sum_{\mathbf{q},\mathbf{q}' \in \mathbb{K}} \kappa_b |\mathbf{q}|^2 |\mathbf{q}'|^2 \bar{h}_{\mathbf{q}} \bar{h}_{\mathbf{q}'} \delta(\mathbf{q}, -\mathbf{q}') \\ &= \frac{L^2}{2} \sum_{\mathbf{q} \in \mathbb{K}} \kappa_b |\mathbf{q}|^4 \bar{h}_{\mathbf{q}} \bar{h}_{-\mathbf{q}} \\ &= \frac{L^2}{2} \sum_{\mathbf{q} \in \mathbb{K}} \kappa_b |\mathbf{q}|^4 |\bar{h}_{\mathbf{q}}|^2 \end{aligned} \tag{17}$$

in which we used the orthogonality property of the Fourier transformations. Equipartition theorem states that the ensemble average of elastic energy for each mode of fluctuations is equal to $\frac{1}{2}kT$. Therefore, the ensemble average of the self correlation function in each mode is obtained as[1]:

$$\langle |\bar{h}_{\mathbf{q}}|^2 \rangle = \frac{kT}{L^2 \kappa_b |\mathbf{q}|^4} \tag{18}$$

Further, for a periodic geometry, since the two-point correlation function is translationally and rotationally invariant, it only depends on the distance between the two points, $r = |\mathbf{r}| = |\mathbf{x} - \mathbf{x}'|$, rather than their positions $(\mathbf{x}, \mathbf{x}')$:

$$\begin{aligned} \langle h(\mathbf{x}) h(\mathbf{x}') \rangle &= \sum_{\mathbf{q},\mathbf{q}' \in \mathbb{K}} \langle \bar{h}_{\mathbf{q}} \bar{h}_{\mathbf{q}'} \mathrm{e}^{\imath(\mathbf{q}\cdot\mathbf{x} + \mathbf{q}'\cdot\mathbf{x}')} \rangle \\ &= \sum_{\mathbf{q},\mathbf{q}' \in \mathbb{K}} \mathrm{e}^{\imath(\mathbf{q}\cdot\mathbf{x} + \mathbf{q}'\cdot\mathbf{x}')} \langle \bar{h}_{\mathbf{q}} \bar{h}_{\mathbf{q}'} \rangle \\ &= \sum_{\mathbf{q} \in \mathbb{K}} \mathrm{e}^{\imath\mathbf{q}\cdot(\mathbf{x}-\mathbf{x}')} \langle |\bar{h}_{\mathbf{q}}|^2 \rangle \delta(\mathbf{q}, -\mathbf{q}') \\ &= \frac{kT}{L^2 \kappa_b} \sum_{\mathbf{q} \in \mathbb{K}} \frac{\mathrm{e}^{\imath\mathbf{q}\cdot\mathbf{r}}}{|\mathbf{q}|^4} \end{aligned} \tag{19}$$

[1]Also note that the modes are decoupled, i.e.

$$\langle h_{\mathbf{q}} h_{\mathbf{q}'} \rangle = \langle |h_{\mathbf{q}}|^2 \rangle \delta(\mathbf{q}, -\mathbf{q}')$$

which is clearly independent of the position of the two points. Similarly, the self correlation function $\langle h^2(\mathbf{x})\rangle$ is independent of the position and is the phase *and* spatial average of $h^2(\mathbf{x})$:

$$\begin{aligned}\langle h^2\rangle &= \langle h^2(\mathbf{x}_1)\rangle = \langle h^2(\mathbf{x}_2)\rangle \\ &= \frac{1}{L^2}\int_{\Omega^{\mathrm{P}}}\langle h^2(\mathbf{x})\rangle = \frac{kT}{L^2\kappa_b}\sum_{\mathbf{q}\in\mathbb{K}}\frac{1}{|\mathbf{q}|^4}\end{aligned} \tag{20}$$

As it can be seen the periodic boundary conditions, dramatically simplify our calculations, and give us closed form expressions for the fluctuations which only depends on the bending modulus. The expression in (18) has been used to extract the bending stiffness of fluid membranes from molecular dynamic simulations. In real cases, however, the fluctuations can be affected by different geometry and boundary conditions. Further, the periodic boundary conditions, automatically remove the contributions from Gaussian modulus and edge properties, (κ_s, ϕ_0), since these parameters enters the equations only through boundary conditions. The statistical mechanics of a system, influenced by a set of boundary conditions, is hard to handle within conventional approaches. Generally, the partition function Z—from which one can obtain the ensemble averages $\langle\mathbb{X}\rangle$ and the free energy F— is defined as:

$$\begin{aligned}Z &= \int \mathrm{e}^{-F[h]/kT}\mathcal{D}[h], \quad F = -kT\log Z, \\ \langle\mathbb{X}\rangle &= \frac{1}{Z}\int \mathbb{X}\,\mathrm{e}^{-F[h]/kT}\mathcal{D}[h]\end{aligned} \tag{21}$$

in which $\mathcal{D}[h]$ denotes integration over all *possible* functions of $h(\mathbf{x})$, that *do satisfy* the boundary conditions. To ensure this, one need to look for the eigenvalues of the associated differential operator ∇^4 for the given geometry and the boundary conditions in (15). Expanding the displacement field in a set of orthogonal eigenfunctions, $u_{m,n}(\mathbf{x})$, one can express the eigenvalue as:

$$\nabla^4 h(\mathbf{x}) = \sum_{m,n}\lambda_{m,n}^4 h_{m,n}u_{m,n}(\mathbf{x}) \tag{22}$$

where $\lambda_{m,n}$ is the eigenvalue associated with the biharmonic operator for the given geometry and boundary conditions. Further, $h_{m,n}$ is the amplitude of

$h(\mathbf{x})$, corresponding to mode (m, n) and is obtained as:

$$h_{m,n} = \frac{1}{A} \int_{\Omega} h(\mathbf{x}) u^*_{m,n}(\mathbf{x}) \tag{23}$$

where A is

$$A = \int_{\Omega} u_{m,n}(\mathbf{x}) u^*_{m,n}(\mathbf{x}) \tag{24}$$

Consequently, the integration in the exponent of the partition function can be written as:

$$\int \frac{1}{2} \kappa_b \left(h \nabla^4 h \right) d\mathbf{x} = \frac{1}{2} \kappa_b A \sum_{m,n} h_{m,n} \lambda^4_{m,n} h^*_{m,n} \tag{25}$$

Using the equipartition theorem, the correlation function then, can be expressed as:

$$\langle h(\mathbf{x}) h(\mathbf{x}') \rangle = \frac{kT}{\kappa_b A} \sum_{m,n} \frac{u_{m,n}(\mathbf{x}) u^*_{m,n}(\mathbf{x}')}{\lambda^4_{m,n}} \tag{26}$$

It is not always, easy and straightforward to obtain a closed-form expression for the eigenvalues and eigenfunctions. In the case of an infinite sheet, for which a periodic boundary conditions is assumed, one can easily obtain the eigenvalues and eigenfunctions, in Fourier space as $\mathbf{q}$ and $e^{\imath \mathbf{q} \cdot \mathbf{x}}$, respectively. However, when the set of admissible functions for h is restricted in the path integration of the partition function, the eigenvalues and eigenfunctions should be solved for the given set of boundary conditions. Alternatively, one can solve for the Green's function in terms of the same eigenvalue and eigenfunctions:

$$G(\mathbf{x}, \mathbf{x}') = \sum_{m,n} G_{m,n}(\mathbf{x}') u_{m,n}(\mathbf{x}) \tag{27}$$

$$\begin{aligned} \kappa_b \nabla^4 G(\mathbf{x}, \mathbf{x}') &= \sum_{m,n} \lambda^4_{m,n} G_{m,n}(\mathbf{x}') u_{m,n}(\mathbf{x}) \\ &= \delta(\mathbf{x}, \mathbf{x}') = \sum_{m,n} u_{m,n}(\mathbf{x}) u^*_{m,n}(\mathbf{x}') \end{aligned} \tag{28}$$

from which we obtain:

$$G_{m,n}(\mathbf{x}') = \frac{u^*_{m,n}(\mathbf{x}')}{\kappa_b \lambda^4_{m,n}} \tag{29}$$

$$\begin{aligned} G(\mathbf{x},\mathbf{x}') &= \sum_{m,n} G_{m,n}(\mathbf{x}') u_{m,n}(\mathbf{x}) \\ &= \sum_{m,n} \frac{u_{m,n}(\mathbf{x}) u^*_{m,n}(\mathbf{x}')}{\kappa_b \lambda^4_{m,n}} \end{aligned} \tag{30}$$

which is exactly what we have in the summation of (26). Therefore, the correlation functions can be easily written in terms of the Green's function as:

$$\langle h(\mathbf{x}) h(\mathbf{x}') \rangle = \frac{kT}{A} G(\mathbf{x},\mathbf{x}') \tag{31}$$

In order to study the statistical mechanics of a system, influenced by a set of boundary conditions, one may choose to *either* evaluate the eigenvalues and eigenfunctions or derive the Green's function in its closed form, rather than the series form in (29)

4. Fluctuations of a free edge

We use the derivation in the preceding section to derive the correlations function for a free edge. Consider a membrane of size L^2, with a free edge and a clamped (opposite) edge. Our goal is to study the fluctuations of the membrane at (and near) the free edge (and far enough from the other three edges), where the contributions of the edge parameters and Gaussian modulus are important. In order to make analytical progress, we model this case with a semi-infinite sheet, with one free edge, to make sure that the fluctuations of the free edge is not affected by the other edges' conditions. Now, consider a semi-infinite sheet embedded in the domain $\Omega^1 := [\mathbf{x} = (x, y); -\infty < x < 0, -\infty < y < \infty]$, having a free edge at $\partial\Omega^1 := [\mathbf{x} = (0, y); -\infty < y < \infty]$. Therefore, we have periodic boundary conditions only in y direction. For this case the boundary conditions in (15) reduce to:

$$\kappa_b \nabla^2 h + \kappa_G \frac{\partial^2 h}{\partial y^2} = 0, \quad \mathbf{x} \in \partial\Omega^1 \tag{32}$$

$$\frac{\partial}{\partial x}\left(\kappa_b \nabla^2 h - \kappa_G \frac{\partial^2 h}{\partial y^2}\right) + \phi_0 \frac{\partial^2 h}{\partial y^2} - \kappa_s \frac{\partial^4 h}{\partial y^4} = 0, \quad \mathbf{x} \in \partial\Omega^1 \tag{33}$$

The Green's function for the given geometry and the above set of boundary conditions is given by the solution of

$$\kappa_b \nabla^4 G(\mathbf{x}, \mathbf{x}') = \delta(\mathbf{x}, \mathbf{x}') \tag{34}$$

Again, due to the translational invariance in the y-direction, $y - y'$ may be substituted for r and derivatives with respect to y and y' may be combined to be considered as derivatives with respect to r. Therefore, the Green's function and its boundary conditions (32), and (33) can be written as:

$$\kappa_b \nabla^4 G(x, x', r) = \delta(x - x')\delta(r) \tag{35}$$

$$\kappa_b \nabla^2 G(x, x', r) + \kappa_G \frac{\partial^2 G(x, x', r)}{\partial r^2} = 0, \quad \mathbf{x} \text{ (or } \mathbf{x}') \in \partial\Omega^1 \tag{36}$$

$$\begin{aligned} &\frac{\partial}{\partial x}\left(\kappa_b \nabla^2 G(x, x', r) - \kappa_G \frac{\partial^2 G(x, x', r)}{\partial r^2}\right) \\ &\quad + \phi_0 \frac{\partial^2 G(x, x', r)}{\partial r^2} - \kappa_s \frac{\partial^4 G(x, x', r)}{\partial r^4} = 0, \quad \mathbf{x} \text{ (or } \mathbf{x}') \in \partial\Omega^1 \end{aligned} \tag{37}$$

The preceding boundary condition equations, (36) and (37), are actually a set of four equations. Two equations when $x = 0$ and $x' \neq 0$ and two equations for when $x' = 0$ and $x \neq 0$. Now, the full set of equations, (35),(36), and (37), will need to be solved.

The first step to solving this set of differential equations is to find a particular solution which satisfies the equation and boundary conditions. This can be done by finding a solution to the infinite system by first taking the Fourier transform of (35) to go from $r \to q$ and $x \to k$ which leads to

$$\kappa_b (k^2 + q^2)^2 G(q, k, x') = \mathrm{e}^{-ikx'} \tag{38}$$

In this context the current definitions of the Fourier and inverse Fourier transforms are given by

$$G(q,x,x') = \frac{1}{L}\int \mathrm{e}^{-iqr} G(r,x,x')\,dr \tag{39}$$

$$G(r,x,x') = \frac{1}{2\pi}\int \mathrm{e}^{iqr} G(q,x,x')\,dq \tag{40}$$

where L is the length of the edge. Taking the inverse Fourier transform as defined in (40) to return from $k \to x$ gives

$$G_P(q,x,x') = \frac{1}{2\pi}\int \frac{\mathrm{e}^{ik(x-x')}}{\kappa_b(k^2+q^2)^2}\,dk \tag{41}$$

This equation can now be solved simply using residue theorem to obtain the particular solution

$$G_P(q,x,x') = \frac{1}{4\kappa_b q^3}\mathrm{e}^{-q|x-x'|}(1+q|x-x'|) \tag{42}$$

This solution was derived to satisfy (35) but also must satisfy the boundary conditions. To check that (36) and (37) are satisfied, both must undergo multiple Fourier transforms to go from $r \to q$. In fact, it is useful to apply the Fourier transform from $r \to q$ to reduce the entire problem to a fourth order ordinary differential equation where only derivatives with respect to x (or x') occur. After transformation the boundary conditions can be written as

$$\frac{\partial^2 G}{\partial x^2} - q^2(1+\alpha)G = 0 \quad \mathbf{x}\,(\text{or } \mathbf{x}') \in \partial\Omega^1 \tag{43}$$

$$\frac{\partial^3 G}{\partial x^3} + q^2(\alpha-1)\frac{\partial G}{\partial x} - f(q)G = 0 \quad \mathbf{x}\,(\text{or } \mathbf{x}') \in \partial\Omega^1 \tag{44}$$

where α is $\bar{\kappa}/\kappa_b$ and

$$f(q) = \frac{\kappa_s}{\kappa_b}q^4 + \frac{\phi_0}{\kappa_b}q^2$$

and all primes denote a derivative with respect to x (or x'). From here, by taking the proper derivatives of (42) and substituting them into the transformed boundary conditions, it is clear that the particular solution does not satisfy the boundary conditions.

Now that a particular solution to the problem has been found, it is necessary to find the homogeneous solution to the problem. To do so, equation (35) will also need to be transformed and set equal to zero, leading to

$$\frac{\partial^4 G}{\partial x^4} - 2q^2 \frac{\partial^2 G}{\partial x^2} + q^4 G = 0 \tag{45}$$

The characteristic equation of (45) shows that the differential equation has two two-fold real roots at $\pm q$. Therefore the solution will be some linear combination of

$$\mathrm{e}^{qx},\ x\mathrm{e}^{qx},\ \mathrm{e}^{-qx},\ x\mathrm{e}^{-qx} \tag{46}$$

Since the out-of-plane fluctuations of the membrane cannot go to infinity as x goes to negative infinity (recall that the domain of x is from $-\infty \to 0$), any solution from (46) that does so may be eliminated. This removes any possible solution with a negative exponent since x is always negative. The solution must also satisfy the boundary equations for both x and x', therefore the homogeneous solution to the problem may be written as

$$G_H = (A\mathrm{e}^{qx} + Bx\mathrm{e}^{qx})(C\mathrm{e}^{qx'} + Dx'\mathrm{e}^{qx'}) \tag{47}$$

Taking the total solution, given by $G = G_P + G_H$, the coefficients A, B, C, and D can be found by substituting into the boundary conditions (43) and (44) and solving the set of four equations simultaneously. Recall That each boundary condition may be used as two equations: once when $x = 0$ and derivatives are taken with respect to x, and once when $x' = 0$ and derivatives are taken with respect to x'. Before solving for these coefficients, it is useful to rewrite the full solution in a new form by expanding the homogeneous solution and grouping like terms. The full solution can then be written as

$$\begin{aligned} G(x, x', q) = {} & \frac{1}{4\kappa_b q^3}\mathrm{e}^{-q|x-x'|}(1 + q|x - x'|) \\ & + (A + Bx + Cx' + Dxx')\,\mathrm{e}^{q(x+x')} \end{aligned} \tag{48}$$

where A, B, C, and D are regrouped coefficients which differ slightly from those in (47), but still remain constant with respect to x. Taking the proper derivatives of (48) with respect to x and substituting into equations (43) and (44) and simplifying gives the following set of equations:

$$\begin{aligned} \frac{-2-\alpha}{4\kappa_b q} + \frac{\alpha x'}{4\kappa_b} + 2q[B + Dx'] - q^2\alpha[A + Cx'] = 0 \\ \mathbf{x} \in \partial\Omega^1 \end{aligned} \tag{49}$$

$$\frac{-2-\alpha}{4\kappa_b q}+\frac{\alpha x}{4\kappa_b}+2q[C+Dx]-q^2\alpha[A+Bx]=0$$
$$\mathbf{x}' \in \partial\Omega^1 \tag{50}$$

$$\frac{2+q\alpha x'}{4\kappa_b}+(2+\alpha)q^2(B+Dx')+(q^3\alpha-f(q))[A+Cx']$$
$$-\frac{f(q)}{4\kappa_b q^3}(1-qx')=0, \qquad \mathbf{x} \in \partial\Omega^1 \tag{51}$$

$$\frac{2+q\alpha x}{4\kappa_b}+(2+\alpha)q^2(C+Dx)+(q^3\alpha-f(q))(A+Bx)$$
$$-\frac{f(q)}{4\kappa_b q^3}(1-qx)=0, \qquad \mathbf{x}' \in \partial\Omega^1 \tag{52}$$

Solving this set of equations simultaneously for the unknown coefficients gives

$$A=\frac{1}{4\kappa_b q^3}\frac{2f(q)-q^3(8+4\alpha+\alpha^2)}{M} \tag{53}$$

$$B=C=\frac{1}{4\kappa_b q^3}\frac{q(\alpha^2q^3-2f(q))}{M} \tag{54}$$

$$D=\frac{1}{4\kappa_b q^3}\frac{-q^2(2\alpha^2q^3)}{M} \tag{55}$$

where

$$M=\alpha(4+\alpha)q^3-2f(q) \tag{56}$$

The final solution with all coefficients in place can now be written as

$$G(x,x',q)=\frac{1}{4\kappa_b q^3}\mathrm{e}^{-q|x-x'|}(1+q|x-x'|)$$
$$+\frac{1}{4\kappa_b q^3}\mathrm{e}^{q(x+x')}\big[U+Vq(x+x')-Wq^2xx'\big] \tag{57}$$

where

$$U=\frac{1}{M}(2f(q)-q^3(8+4\alpha+\alpha^2)) \tag{58}$$

$$V=\frac{1}{M}(\alpha^2q^3-2f(q)) \tag{59}$$

$$W = \frac{1}{M}(2\alpha^2 q^3) \tag{60}$$

Taking the values along edges $\mathbf{x} = \mathbf{x}' = (0, y)$, gives us the self correlation of the edge in Fourier space as:

$$\langle |h(q)|^2 \rangle = \frac{kT}{L} G(0, 0, q) \tag{61}$$

5. MD simulation of free edge of a lipid membrane

Typically, molecular dynamics of lipid membranes is performed on a small patch with edges or an "infinite" membrane using periodic boundary conditions. Here, the goal is to simulate a lipid membrane in a "semi-infinite" configuration. Meaning that the membrane has only one free edge (previously defined as the edge at $x = 0$) and extends infinitely in all other in-plane directions. Of course, molecular dynamics, nor any other type of simulation, cannot recreate something that is truely infinite in nature. Thus some manipulations must be made to reach a state that can be thought of as essentially semi-infinte in nature and behavior.

All molecular dynamics simulations performed in this section are done using the freely available software GROMACS, version 4.6.7, with the coarse grained MARTINI force field[3, 4]. The use of the MARTINI force field allows a great simplification of the system as the coarse graining method used combines approximately every 4 heavy atoms into a single bead. This allows the MARTINI force field to simulate much larger systems than other traditional all-atom force fields, with the loss of some detail at the atomic level. Since this work is concerned with long wavelength fluctuations of a membrane edge, the details that are lost are like negligible and most definitely are greatly outweighed by the benefits of using a coarse grained force field. Another such benefit, other than the greater length scale mentioned earlier, is that since several atoms are grouped together and treated as a single bead, essentially a large "atom" with special parameters, is an increase in the accessible time scales. In general all-atom molecular dynamics may only reach time scales of a few nanoseconds due to the small time step required due to the vibrational frequency of individual atoms. By no longer simulating individual atoms, the MARTINI force field may use a time step 10 to 20 times greater than that of an all-atom force field allowing simulations to reach microsecond timescales. This is particularly useful for more slowly undulating

long wavelength fluctuations which will be most important here.

For the simulations here, the chosen lipid is DPPC whose topology is already defined in the MARTINI force field making it reasonable choice. The choice of lipid for this simulation is not of particular importance, as long as it is known to form a stable bilayer. Different lipids will change the membrane properties of interest, but any choice would be fine for a "proof-of-concept" which is the desired outcome of these simulations. A starting configuration of lipids is built by replicating and rotating a single DPPC molecule to create a membrane patch with lengths of approximately 100 nm in the x direction and 100 nm in the y directions. All simulations will use periodic boundary conditions in all directions, but to best recreate a semi-infinite membrane the patch will be continuous in the y direction and an addition 20 nm will be added between the periodic images in the x direction. The z dimension (normal to the bilayer) of the simulation box will be set to a starting value of 20 nm to ensure that there is no interaction with the periodic image in that direction as well. All empty space is then filled with water molecules as solvent; in the MARTINI force field, each water molecule represents 4 real (all-atom) water molecules. The total system includes 15,120 DPPC molecules and nearly 800,000 MARTINI water molecules.

After building the starting structure, the energy of the system is minimized using the steepest descents algorithm until the maximum force on any single atom is less than 100 $kJ \cdot mol^{-1} \cdot nm^{-1}$. This minimization is done in two steps, first with all of the DPPC molecules restrained to remove any bad contacts from adding the water molecules to the system, and then again with the entire system subject to energy minimization. After energy minimization, a stable membrane structure has been created.

The following simulations will be done under the NPT ensemble with isotropic pressure coupling based on the velocity-rescaling thermostat and Berendsen barostat to maintain a constant temperature of 323 K and pressure of $1bar$. An NPT ensemble is used over other choices, like NVT, to allow the simulation of a tension free bilayer. Since no pressure or temperature are introduced during the energy minimization, the system now needs to be somewhat equilibrated before reasonable results can be obtained. The equilibration also take place in two stages. First a small timestep of 2 fs is used for 200,000 steps; this allows the bilayer to form proper edges which will

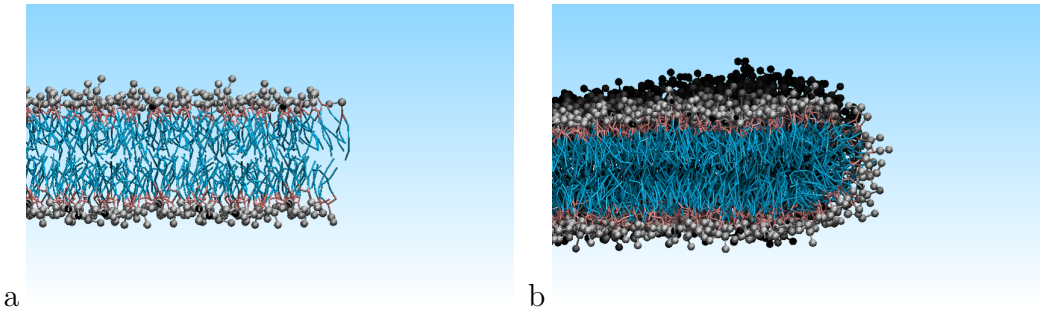

Figure 2: Emphasis on the structure of the bilayer edge (a) before equilibration and (b) after equilibration.

not allow the hydrophobic core to be exposed to the solvent molecules, as in the starting configuration. The timestep is now increased to the value which will be used for the remainder of the simulations; this time step is 20 fs and the last equilibration simulation is run for 100,000 steps.

Until now, no mention of how the bilayer will recreate a semi-infinite membrane has been made. If the equilbration simulations were allowed to continue as previously described for a sufficient amount of time, the bilayer would tend to fluctuate and slowly reshape into an infinite membrane. This is due to the fact that an NPT ensemble was chosen, allowing the simulation box size to change to maintain a constant pressure. The fluctuations in box size will then allow the membrane to move to the minimum energy state where no rounded edges like the one shown in Figure 2 exist. Therefore, some constraint needs to be added to prevent this from happening. The added constraint on the system is achieved by "clamping" one edge of the bilayer; the clamped edge is parallel to the y axis so that the free edge is 100 nm away, ideally much further than the persistence length of the membrane constraints. The clamping is done in GROMACS by adding a constraint to the DPPC molecules on one edge of the bilayer. This constraint acts as a harmonic potential, essentially a spring, whose equilibrium position is the starting position of the atom so that large movements of the clamped atoms come with a heavy energy penalty. The value of these spring constants are set to $1,000\ kJ \cdot mol^{-1} \cdot nm^{-1}$, and applied on all degrees of freedom for the clamped atoms. Another small equilibration simulation is run for 500,000 steps with a timestep of 2 fs to allow the system to adjust to the

new constraints. Before running any simulations from which data will be used one last simulation is run for 500,000 steps with the larger timestep of 20 fs and the constraints. Finally, a simulation is run for 2,500,000 steps with a 2 fs timestep for a total simulation length of 50 ns from which the necessary edge fluctuation data can be extracted. The same procedure is repeated for two additional bilayers composed of DOPC and DOPE lipids for comparison.

It is also necessary to find the bending modulus of each bilayer. Many methods to do so have been well documented including thermal fluctuation spectra, buckling, and lipid orientation fluctuations [5, 6, 7]. The method chosen to calculate the bending modulus here is using the thermal fluctuation spectra for each of the different lipid types. A comprehensive resource on the implementation of this method was detailed by Brandt et al. in 2011 [8]. To obtain the fluctuation data for this procedure a periodic bilayer was created for each of the three lipid types previously used (DPPC, DOPC, DOPE). Each structure contained 7,200 lipid molecules to create a lipid patch of roughly 50 $nm \times 50\,nm$. Data is extracted from simulations done over 220 ns after equilibration, and the results are summarized in Table 1. These results are in good agreement with other recently published values of the bending moduli obtained using different methods which are also included in the table.

Table 1: Summary of bending modulus values found in present work and comparison with other sources. The various methods are abreviated as Fluctuation Spectra (FS), Orientation Fluctuations (OF), and Buckling (BU)

Lipid Type	Force Field	κ_b (k_BT)	Method	Source
DPPC	MARTINI	36.0	FS	Present Work
DPPC	CHARMM36	35.0	OF	[9]
DPPC	MARTINI	32.7	BU	[10]
DOPC	MARTINI	28.7	FS	Present Work
DOPC	CHARMM36	25.6	OF	[9]
DOPC	MARTINI	21.5	BU	[10]
DOPE	MARTINI	22.4	FS	Present Work

6. MD simulations of free edge of a graphene sheet

Graphene monolayer has been recognized as a solid membrane, where the in and out-of-plane deformations are coupled. The kinematic of the

deformation in solid membranes is analogous to von-Karman plate theory. Let $\mathbf{u}$ and h be the in and out-of-plane displacement fields, respectively. Then the in-plane strain field is defined as:

$$\varepsilon_{\gamma\delta} = \frac{1}{2}\left(\frac{\partial u_\gamma}{\partial x_\delta} + \frac{\partial u_\delta}{\partial x_\gamma} + \frac{\partial h}{\partial x_\gamma}\frac{\partial h}{\partial x_\delta}\right) \tag{62}$$

Having the strain field in (62), the resulting stress tensor can be written as:

$$\sigma_{\gamma\delta} = \frac{E}{1-\nu^2}\left(\varepsilon_{\gamma\delta} + \frac{\nu}{1-\nu}\varepsilon_{kk}\delta_{\gamma\delta}\right) \tag{63}$$

where E and ν are the elastic Young modulus and poisson ratio of the graphene sheet, respectively. Then, using the above stress field and the strain field in (62), the in-plane strain energy can be written as:

$$U_s = \int \frac{1}{2}\sigma_{\gamma\delta}\varepsilon_{\gamma\delta} \tag{64}$$

which implies that even in the absence of the in-plane motions—where $\mathbf{u} = 0$—the out-of-plane deformations results in a *quartic* stretching energy. The total energy is the summation of the bending energy and the stretching energy in (64). Due to the nonlinear contribution of the stretching energy, the thermal fluctuations of graphene monolayers are not analytically obtainable even for an infinite sheet, with no boundaries. MD simulations of graphene monolayers, with periodic boundary conditions in all directions, show that the apparent bending stiffness of graphene at finite temperature is much larger than its bare value—at zero kelvin. This can be physically explained by the fact that graphene's in-plane Young's modulus is relatively high that at finite temperature, suppresses the fluctuations—due to nonlinearities. Consequently, the bare value of graphene monolayers are all reported at zero kelvin. At finite temperature, depending on the size of the sheet and the temperature, graphene monolayers exhibit stiffening with various intensities.

In this work, the linear elasticity gives us an estimate of the mechanical properties. To minimize the effects arising from nonlinearities, we perform MD simulations under NPT ensemble to relax the in-plane stress field as much as possible.

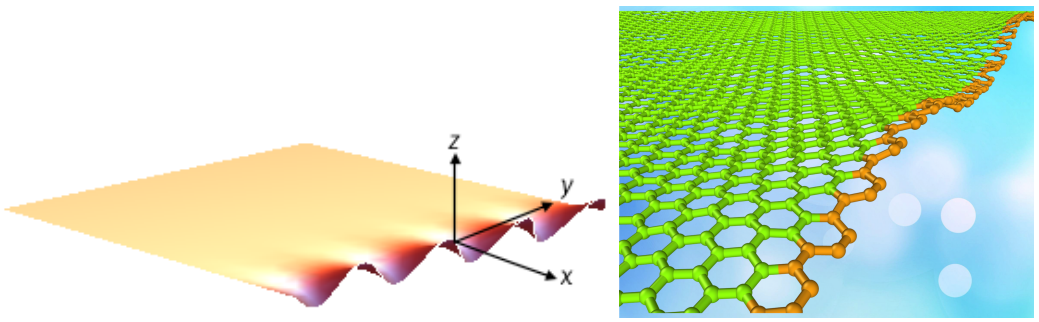

(a) (b)

Figure 3: (a): Schematic of the geometry and boundary conditions used in this model. The 2D elastic sheet has only one free edge with periodic boundary condition. (b): Snapshot of edge fluctuations of graphene in MD simulations. The atoms at the free edge are shown in different color and their heights are used to in analyzing the edge fluctuations.

We perform MD simulations of monolayer graphene using LAMMPS, an open source code[11]. The second- generation reactive empirical bond-order (REBO) potential[12] is used for the multibody C–C interactions in graphene. The temperature is controlled by a Nose-Hoover thermostat. Each simulation runs up to 20 ns (time step: 1 fs), with the first 10 ns for the system to equilibrate and the subsequent 10 ns for calculations of the time-averaged quantities. The time integration scheme closely follows the time-reversible measure-preserving Verlet and rRESPA integrators derived by Tuckerman et. al.[13]. In order to avoid interlayer interactions, relatively thick simulation boxes are used (thickness 24.5 nm). We performed the simulations for both armchair and zigzag free edges. Graphene monolayer, with a free edge undergoes relatively large fluctuations. Beyond a certain size scale the free edge becomes unstable and undergoes folding and rotating around the clamped edge. In order to stabilize the free edge a slightly different boundary condition is used for graphene, compared to lipid bilayers. The schematic is shown in Figure 3 where three edges are fixed and one edge is allowed to freely fluctuate. To model the simply supported edges, only one row of the atoms on the edge is fixed. For the clamped edge, more than one row of atoms should be fixed to satisfy the boundary conditions on both displacement field (h) as well as the gradient of the displacement field (∇h). While this geometry stabilizes the free edge, it doesn't add much complexity to our theoretical calculations. In the following we explain how these boundary conditions should be carefully accounted for in transforming the data into

Fourier space.

7. Results

Table 2: Estimated values for Gaussian modulus and edge properties at finite temperature, for different kinds of lipid and graphene.

2D material	κ_b	κ_G	ϕ_0	κ_s
DPPC	36 k_BT	-28.8 k_BT	59 pN	-10.8 k_BT
DOPC	28.7 k_BT	-2.87 k_BT	68 pN	-14.3 k_BT
DOPE	22.4 k_BT	-2.24 k_BT	74 pN	-11.2 k_BT
Graphene	1.5 eV	25 meV	1 eV/nm	0

With the simulations complete, the data along the edge must undergo a discrete Fourier transform defined by

$$h(q) = \frac{1}{N}\sum_{k=1}^{N} z(0, y_k)e^{-iqy_k}\,, \tag{65}$$

where N is the number of data points along the edge, $z(0, y_k)$ is the height fluctuation, and q is given by $q = 2\pi mL^{-1}$ with $m = 0, 1, 2, ...$ The transformed fluctuation spectrum can then be related to the Green's function by (61).

For lipid membrane, to take the Fourier transform of the free edge, all of the atomic coordinates of the membrane withing 5 nm of the edge are output for analysis. The y-direction, parallel to the free edge, is then broken up into several bins of consistent size; the number of bins is equal to N in (65). This ensures that data will be fairly evenly spaced along the edge. The coordinates for each bin are found by taking the average coordinates of all membrane atoms within 1 nm of the edge; the mean z-coordinate is subtracted to get the necessary values for $z(0, y_k)$ such that

$$\sum_{k=1}^{N} z(0, y_k) = 0\,. \tag{66}$$

With the Fourier transformed data, the solution $G(0, 0, q)$ is fit to the data using a least squares fit to find the optimized values for the Gaussian modulus, edge modulus, and edge tension.

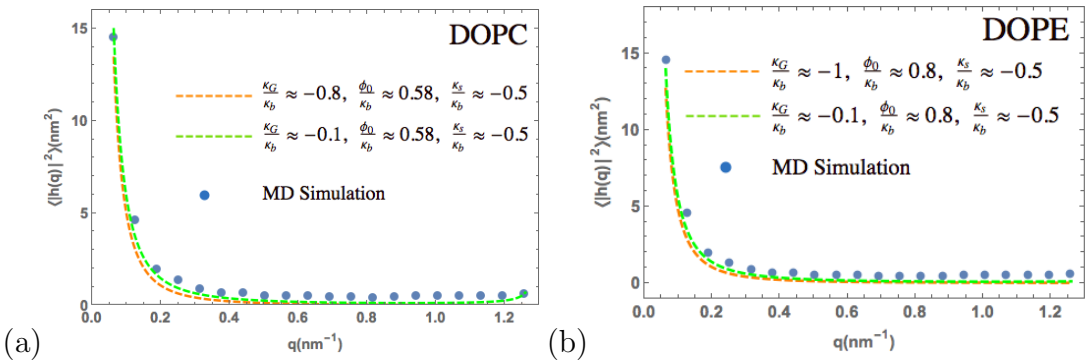

Figure 4: Fitting data from MD simulations to two types of lipid membranes. The blue dotted data are calculated by transforming the data from MD simulation into Fourier space. The bending modulus κ_b is separately calculated from thermal fluctuations of a patch of membrane under periodic boundary conditions in all directions. The corresponding values are reported in Table 1. In the plot, the green dashed line gives us a better fit compared to the dashed orange line.

Other than DPPC, discussed in the paper, we explored the edge properties and Gaussian modulus for two other types of lipid membranes, DOPC and DOPE. The results are shown in Figure 4. Our results show that typical values of Gaussian modulus $\kappa_G \sim -\kappa_b$ cause discrepancies between the fitted curve and the MD data. This suggests further revision of estimation of Gaussian modulus in experiments and atomistic methods. Further, the edge modulus having a negative value appeared to provide a better fit compared to positive values. The edge modulus captures the excess bending energy at the free edge. Accordingly, $\kappa_s/\kappa_b \approx -0.5$ suggests that the bending modulus at a free edge is roughly half of the bending modulus at the rest of the membrane. This of course can be do to the re-orientation of lipid molecules at the free edge to block the entrance of solvent into the membrane.

For graphene monolayer, since we have used a different boundary conditions, the Fourier transform of the data is not the same as (65). In fact, in each mode, we can have either $\sin(qy)$ *or* $\cos(qy)$ and *not both* of them. Let the length of the free edge be $2L$ expanded in the domain $-L < y < L$ and $q = \pi m/L$. Then the deformation modes have to satisfy $h(L) = h(-L) = 0$. Hence, we cannot have eigenfunctions such as $\cos(2\pi ny/2L)$ or $\sin((2n-1)\pi x/2L)$. Accordingly, for odd (even) values of m, we only used $\sin(m\pi y/L)$ ($\sin(m\pi y/L)$). In general one can expand the

Green's function in terms of sin(qx) and cos(qx) functions:

$$G(x,x',y,y') = f(x,x',y') \sum_q (a_q \sin(qy) + b_q \cos(qy)) \tag{67}$$

where $q = \frac{m\pi}{2L}$. Let the free edge expand in $(-L < x < L)$. Now, for simply supported condition at $x = \pm L$, we need to satisfy $G = 0$. Therefore, if $m = 1, 3, 5, \cdots$, then $a_q = 0$, and if $m = 2, 4, 6, \cdots$, then $b_q = 0$.

Consider an even mode, i.e. $m = 2, 4, 6, \cdots$. Substituting the Fourier expansion into the differential equation we obtain:

$$\begin{aligned}
\kappa_b \nabla^4 G(x,x',y,y') &= \delta(x-x')\delta(y-y') \\
\kappa_b (k^2+q^2)^2 G(k,x',q,y') &= \mathrm{e}^{-ikx'} \sin(qy') \\
G_P(q,y',x,x') &= \frac{1}{2\pi} \int \frac{\sin(qy')\mathrm{e}^{ik(x-x')}}{\kappa_b (k^2+q^2)^2}\, dk \\
G_P(q,y',x,x') &= \frac{\sin(qy')}{4\kappa_b q^3} \mathrm{e}^{-q|x-x'|}(1+q|x-x'|)
\end{aligned} \tag{68}$$

The final solution with all coefficients in place can now be written as

$$\begin{aligned}
G(x,x',q,y') = &\frac{\sin(qy')}{4\kappa_b q^3} \mathrm{e}^{-q|x-x'|}(1+q|x-x'|) \\
&+ \frac{\sin(qy')}{4\kappa_b q^3} \mathrm{e}^{q(x+x')} \left[U + Vq(x+x') - Wq^2 xx'\right]
\end{aligned} \tag{69}$$

where

$$M = \alpha(4+\alpha)q^3 - 2f(q) \tag{70}$$

$$\begin{aligned}
U &= \frac{1}{M}(2f(q) - q^3(8+4\alpha+\alpha^2)) \\
V &= \frac{1}{M}(\alpha^2 q^3 - 2f(q)) \\
W &= \frac{1}{M}(2\alpha^2 q^3)
\end{aligned} \tag{71}$$

$$\begin{aligned}
G(0,0,y,y') &= \sum_q G(0,0,q,y') \sin(qy) \\
&= \sum_q \frac{\sin(qy')\sin(qy)}{4\kappa_b q^3}(U+1)
\end{aligned} \tag{72}$$

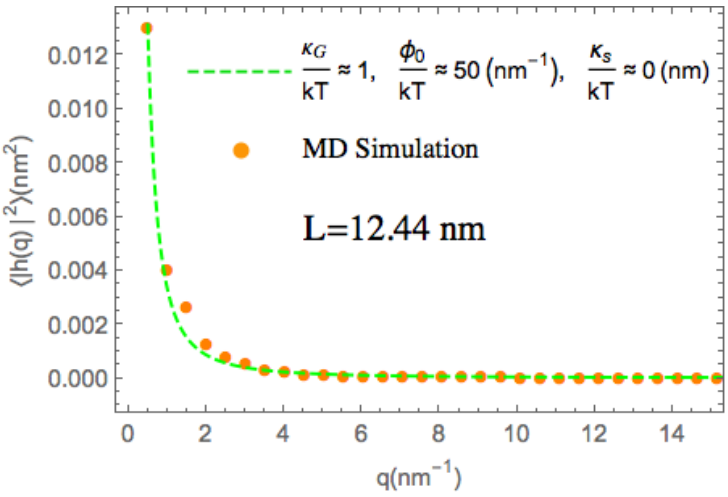

Figure 5: Fluctuations of the free edge of graphene monolayer with size of $L = 12.44nm$.

Taking the solution at the free edge ($x = x' = 0$), back into real space, we have:

$$G(0,0,y,y) = \sum_q \frac{\sin(qy)^2}{4\kappa_b q^3}(U+1) \tag{73}$$

Similarly, one can expand the displacement field in Fourier space:

$$h(0,y) = \sum_q h_q \sin(qy) \tag{74}$$

Then the self correlation function at the free edge is obtained as:

$$\begin{aligned}
\langle h(x=0)^2 \rangle &= \frac{1}{2L}\int \langle h(0,y)^2 \rangle dy \\
&= \frac{1}{2L}\int_{-L}^{L} \sum_{q,q'} \langle h_q h_{q'} \sin(qy)\sin(q'y) \rangle dy \\
&= \frac{1}{2}\sum_q \langle h_q^2 \rangle
\end{aligned} \tag{75}$$

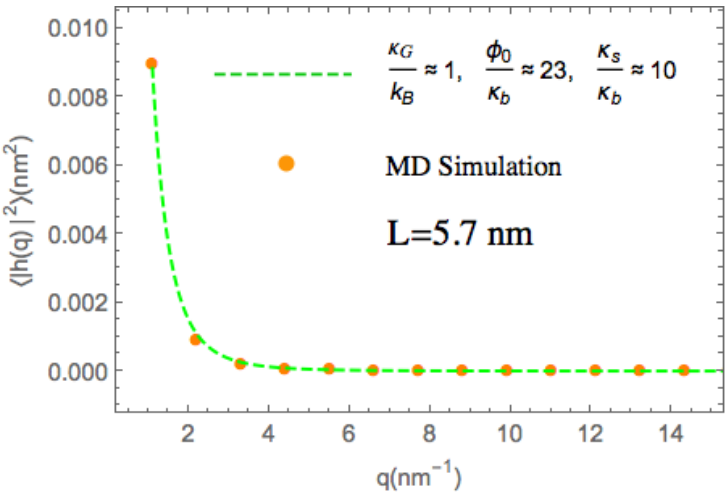

Figure 6: Fluctuations of the free zigzag edge of graphene monolayer with size of $L = 5.7nm$.

The spatial average of the Green's function along the edge is:

$$\begin{aligned}\frac{1}{2L}\int G(0,0,y,y)dy &= \frac{1}{2L}\int_{-L}^{L}\sum_{q}\frac{\sin(qy)^2}{4\kappa_b q^3}(U+1)dy \\ &= \frac{1}{2}\sum_{q}\frac{1}{4\kappa_b q^3}(U+1) \end{aligned} \tag{76}$$

On the other hand, since we have:

$$\langle h(0,y)^2\rangle = \frac{k_B T}{L}G(0,0,y,y), \tag{77}$$

then, one can easily verify that

$$\langle h_q^2\rangle = \frac{k_B T}{4L\kappa_b q^3}(U+1) \tag{78}$$

Same can be shown for odd modes, with cos(qx), being the only eigenfunction. Therefore, the results in Fourier modes for simply supported boundary condition is not much different from periodic boundary conditions.

The reported values in the paper and in Figure 5, correspond to the armchair edge. We also ran separate simulations for the zigzag edge and the

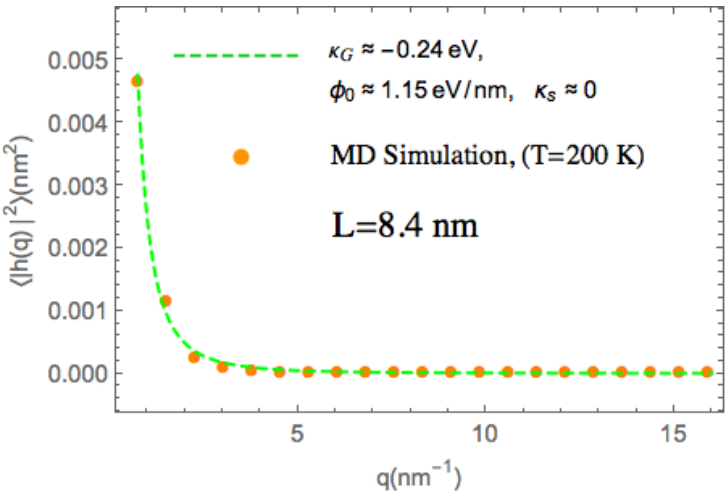

Figure 7: Fluctuations of the free armchair edge of graphene monolayer with size of $L = 8.4nm$ at $T = 200$K.

results are shown in Figure 6. As it can be seen, the Gaussian modulus did not change but (as fully expected) the edge energy and edge modulus are noticeably different. Nevertheless, the edge energy is still a positive value, unlike the reported zero Kelvin values.

Other than values reported in the paper, we also explored the size dependency of edge properties and Gaussian modulus. We find that the edge modulus and Gaussian modulus remain unaltered, while the edge tension changes slightly. For a larger edge size $L = 12$ nm, which is 50% larger than the original edge size– 8 nm–, we found that the edge tension changes about 5% which is about 50 meV. Meanwhile, the Gaussian modulus did not show size dependency and remains a small positive value for larger sizes as well.

8. Variation of Gaussian modulus and edge properties of graphene with temperature

In this section, we explore the temperature-dependence of the graphene Gaussian modulus and edge properties. The zero Kelvin values of these properties have been studied in the literature and there appears to be some consensus regarding the sign as well as the order of the properties. A couple of key works appeared in the literature recently to extract the Gaussian modulus of graphene at zero Kelvin.Wei et. al.[14], using quantum calculations,

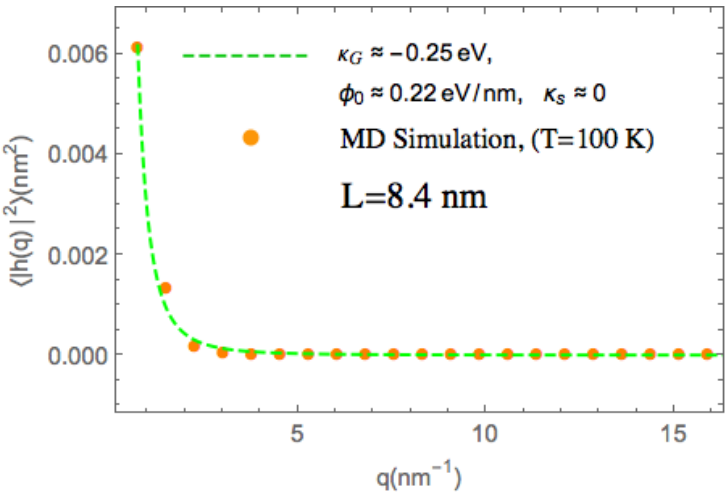

Figure 8: Fluctuations of the free armchair edge of graphene monolayer with size of $L = 8.4nm$ at $T = 100$K.

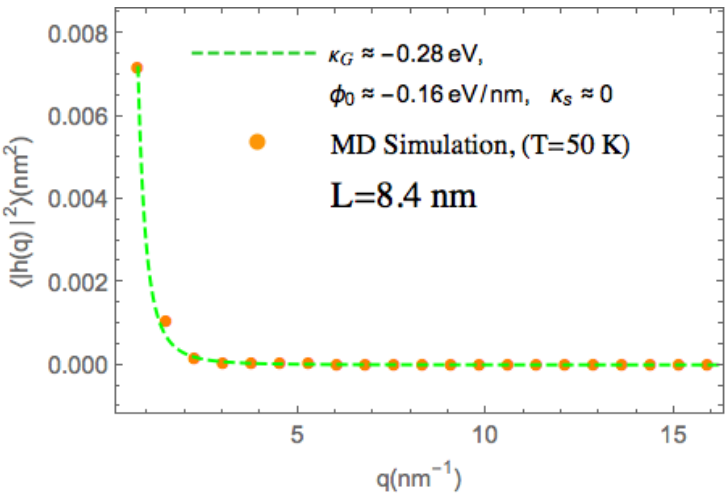

Figure 9: Fluctuations of the free armchair edge of graphene monolayer with size of $L = 8.4nm$ at $T = 50$K.

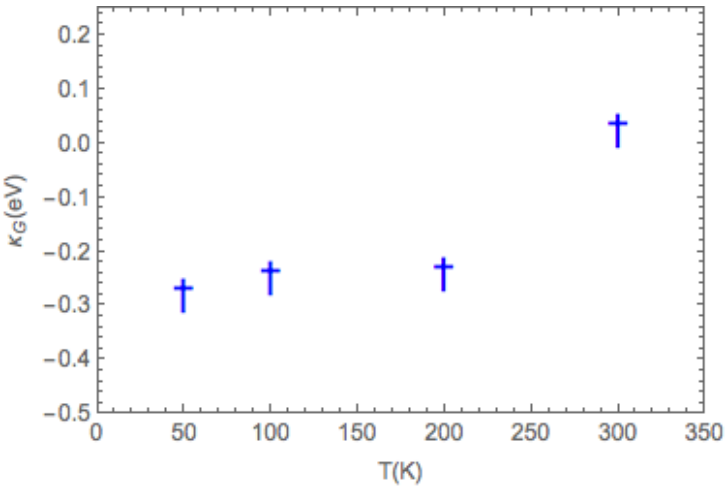

Figure 10: Estimated values of Gaussian modulus at different temperatures.

estimated the Gaussian modulus at zero Kelvin to be ~ -1.52eV by comparing the potential energy of graphene for different topological structures. In a different work, Davini et. al.[15] derived a continuum 2-dimensional model of a graphene sheet and with appropriate linkage with Molecular Dynamics (MD) 2nd-generation reactive empirical bond-order (REBO) potential[12], they estimated the Gaussian modulus at zero Kelvin to be ~ -1.62 eV. At finite temperature, however, we see large discrepancies (both sign and magnitude) for Gaussian modulus, compared to its zero Kelvin value. We therefore expect that as the temperature decrease, the values for Gaussian modulus and edge properties as estimated from our approach should qualitatively tend towards the corresponding zero Kelvin values. To verify this, we ran further simulations at different temperatures $T = 200K$, $T = 100K$, and $T = 50K$. Comparing the results of these simulations we highlight a few points as following:

- The results for $T = 200$ K, $T = 100$ K and $T = 50$ K are shown in Figures 7, 8, and 9, respectively. The corresponding values for the properties are given in each plot. The negative value for Gaussian modulus appeared at $T = 200$ K and after that, further decreasing the temperature, also decreases the Gaussian modulus. The overall decreasing trend is shown in Figure 10.

- In addition to Gaussian modulus, the edge tension also decreases as the

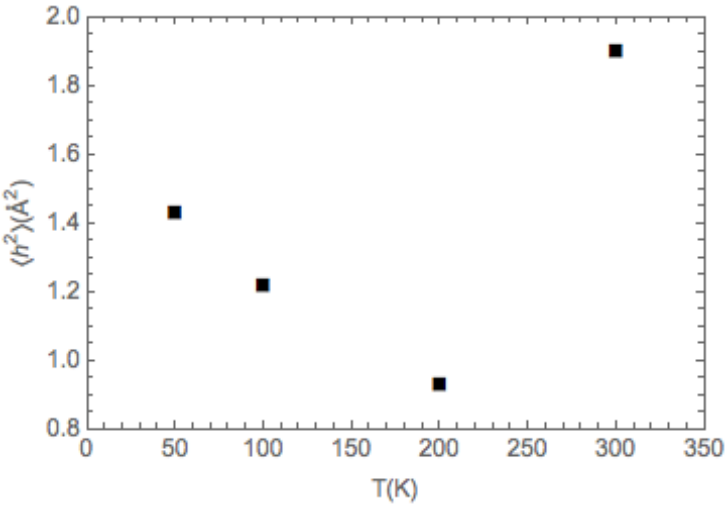

Figure 11: Variation of the amplitude of the out-of-plane deformation with temperature

temperature goes down. Note that, at long wave length, the edge tension determines the amplitude of the fluctuations. At some point, however, the edge tension approaches zero. The fluctuations amplitude— assuming zero edge modulus— is then approximated by:

$$\langle |h(q)|^2 \rangle = -\frac{2kT\kappa_b}{Lq^3\kappa_G\left(4\kappa_b+\kappa_G\right)} - \frac{4kT\kappa_b^2}{Lq^4\kappa_G^2\left(4\kappa_b+\kappa_G\right)^2}\phi_0 \tag{79}$$

which shows that, for positive values of edge tension, the fluctuations should be smaller, compared to negative values. As the temperature decreases, the decreasing trend of edge tension is vividly captured by the increase of fluctuations (this is rather counterintuitive if we are to compare this to an infinite sheet rather than one with an edge). We would expect smaller fluctuations for lower temperature, however, in our MD simulations, the out-of-plane deformations are observed to increase!—results for the square of the amplitude is given in Figure 11. At $T = 200$ K, we observe a subtle transition for fluctuations, which indicates that the edge tension is decreasing. The overall decreasing trend of the edge tension is also given in Figure 12.

- We also note that our theoretical model is based on the assumption that the open edge remains stable on its flat configuration. However, as the temperature approaches zero, the edge undergoes buckling and

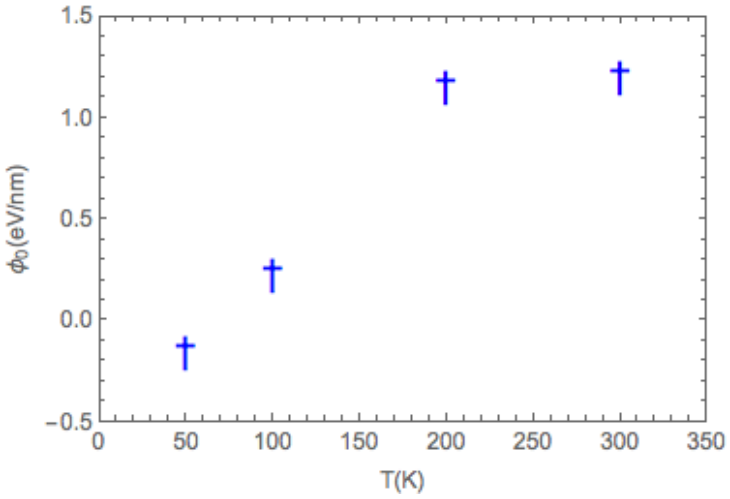

Figure 12: Estimated values of edge tension for different temperatures.

.

is no longer flat. Accordingly, for lower temperature—specially when the edge force reaches negative values, careful consideration is required when fitting and interpreting the data, as in such case, the out-of-plane deformations might be due to buckling instabilities and not fully thermal excitations.

References

[1] A. Biria, M. Maleki, E. Fried, Continuum theory for the edge of an open lipid bilayer, Adv. Appl. Mech 21 (2013) 1–78.

[2] Z. Tu, Z. Ou-Yang, A geometric theory on the elasticity of bio-membranes, Journal of Physics A: Mathematical and General 37 (2004) 11407.

[3] B. Hess, C. Kutzner, D. Van Der Spoel, E. Lindahl, Gromacs 4: algorithms for highly efficient, load-balanced, and scalable molecular simulation, Journal of chemical theory and computation 4 (2008) 435–447.

[4] S. J. Marrink, H. J. Risselada, S. Yefimov, D. P. Tieleman, A. H. De Vries, The martini force field: coarse grained model for biomolecular simulations, The Journal of Physical Chemistry B 111 (2007) 7812–7824.

[5] E. Lindahl, O. Edholm, Mesoscopic undulations and thickness fluctuations in lipid bilayers from molecular dynamics simulations, Biophysical journal 79 (2000) 426–433.

[6] M. Deserno, Fluid lipid membranes: From differential geometry to curvature stresses, Chemistry and physics of lipids 185 (2015) 11–45.

[7] M. C. Watson, E. S. Penev, P. M. Welch, F. L. Brown, Thermal fluctuations in shape, thickness, and molecular orientation in lipid bilayers, The Journal of chemical physics 135 (2011) 244701.

[8] E. G. Brandt, A. R. Braun, J. N. Sachs, J. F. Nagle, O. Edholm, Interpretation of fluctuation spectra in lipid bilayer simulations, Biophysical journal 100 (2011) 2104–2111.

[9] Z. A. Levine, R. M. Venable, M. C. Watson, M. G. Lerner, J.-E. Shea, R. W. Pastor, F. L. Brown, Determination of biomembrane bending moduli in fully atomistic simulations, Journal of the American Chemical Society 136 (2014) 13582–13585.

[10] D. Bochicchio, L. Monticelli, The membrane bending modulus in experiments and simulations: a puzzling picture (2015).

[11] S. Plimpton, Fast parallel algorithms for short-range molecular dynamics, Journal of computational physics 117 (1995) 1–19.

[12] D. W. Brenner, O. A. Shenderova, J. A. Harrison, S. J. Stuart, B. Ni, S. B. Sinnott, A second-generation reactive empirical bond order (rebo) potential energy expression for hydrocarbons, Journal of Physics: Condensed Matter 14 (2002) 783.

[13] M. Tuckerman, B. J. Berne, G. J. Martyna, Reversible multiple time scale molecular dynamics, The Journal of chemical physics 97 (1992) 1990–2001.

[14] Y. Wei, B. Wang, J. Wu, R. Yang, M. L. Dunn, Bending rigidity and gaussian bending stiffness of single-layered graphene, Nano letters 13 (2012) 26–30.

[15] C. Davini, A. Favata, R. Paroni, The gaussian stiffness of graphene deduced from a continuum model based on molecular dynamics potentials, Journal of the Mechanics and Physics of Solids 104 (2017) 96–114.